THE ASTROPHYSICAL JOURNAL, 374:687–699, 1991 June 20

CYCLOTRON RESONANT SCATTERING AND ABSORPTION

ALICE K. HARDING
Laboratory for High Energy Astrophysics, Code 665, NASA/Goddard Space Flight Center, Greenbelt, MD 20771
AND
JOSEPH K. DAUGHERTY
Computer Science Department, University of North Carolina-Asheville, Asheville, NC 28804
Received 1990 August 21; accepted 1990 December 12

ABSTRACT

We have made a detailed comparison of the relativistic cross sections for both first-order absorption and second-order scattering to determine the conditions under which the absorption cross section is a good approximation to the much more complex scattering cross section for purposes of modeling cyclotron lines in gamma-ray bursts. This requires a full treatment of the spin-dependent relativistic natural line widths as well as the derivation of the spin-dependent cross sections. Differences in both the cross sections and the line profiles will be presented for a range of field strengths, angles, and electron temperatures. Although the scattering and absorption cross sections are equal at the resonance energies (to second order in α), we find that their relative difference at one line width from resonance increases with field strength and harmonic number. The difference is also strongly dependent on the photon angle to the magnetic field and can be traced to the fact that resonant scattering does not have a standard Lorentz profile. For the field strength, 1.7×10^{12} G, and angle inferred from the *Ginga* burst features, absorption is an excellent approximation for the profiles at the first and second harmonics. However, scattering cross sections should be used to model lines accurately at higher harmonics and higher field strengths.

Subject headings: gamma rays: bursts — line profiles — radiation mechanisms — relativity

1. INTRODUCTION

The discovery of harmonic absorption features in the spectra of two gamma-ray bursts by detectors on the *Ginga* satellite (Murakami et al. 1988) has provided strong evidence that the cyclotron line interpretation of low-energy dips seen in earlier gamma-ray burst spectra is correct and has intensified theoretical investigations into the physics of cyclotron scattering in strong magnetic fields (Wang et al. 1989; Harding & Preece 1989; Alexander & Mészáros 1989). In the low-density, strongly magnetized plasmas presumed to be present in gamma-ray burst–emitting regions, collisions are unimportant relative to radiative processes (Bussard & Lamb 1982), and almost all of the electrons are in the ground Landau state. Therefore, the absorption of photons at the cyclotron harmonic frequencies by electrons in the ground state is almost always followed by reemission of one or more cyclotron photons, so that resonant scattering is the physically accurate description. However, because the relativistic second-order scattering cross section is quite complex, it is advantageous for numerical modeling of cyclotron lines to use the first-order absorption cross section as an approximation. The physical difference between scattering and absorption is that the second-order scattering description includes a virtual intermediate state which does not require strict energy-momentum conservation at each vertex. The resulting off-mass shell contributions are usually negligible for nonrelativistic processes. However, in the strong magnetic fields above 10^{12} G present near neutron stars, relativistic effects in cyclotron scattering cannot be ignored, and differences between the first- and second-order descriptions may become significant.

In this paper we investigate the behavior of cyclotron resonant scattering and absorption at high magnetic field strengths to determine when absorption is a good approximation to scattering. We also evaluate the errors in the absorption approximation as a function of field strength and angle of the incident photon to the field direction. In the relativistic regime, the natural line width of the cyclotron resonances, determined by the radiative decay rates, is dependent on the spin of the electron. Therefore, the resonances associated with spin-up and spin-down states have different widths. Since the published cross sections for scattering (Herold 1979; Daugherty & Harding 1986; Bussard, Alexander, & Mészáros 1986) are summed over intermediate state spin and those for absorption (Daugherty & Ventura 1978) are summed over final spin state, it is necessary to rederive the spin-dependent parts of the cross sections. The relativistic absorption and scattering cross sections are dependent on photon polarization as well. Although polarization effects are very important in a full resonant transfer calculation of the emergent spectrum (Alexander & Mészáros 1989), we will explore in this paper only properties of the polarization-averaged cross sections. However, expressions for the cross sections are given in their polarization-dependent forms.

In § 2 we give the expressions for the absorption and scattering cross section in the case of electrons at rest in the ground state. Section 3 presents results of a comparison of the scattering and absorption cross sections as a function of photon energy and angle, and of magnetic field strength. We show that the major difference is due to relativistic effects on the shape of the resonant peak, which suggests a possible way of "fixing" the Lorentz profile of the absorption cross section to include these effects. In § 4, we present calculations of the scattering and absorption profiles for one-dimensional thermal electron distributions for three field strengths and photon angles. Finally, we discuss the implications of these results for the modeling of cyclotron lines in astrophysical sources.

2. SCATTERING AND ABSORPTION CROSS SECTIONS

Resonances appear in magnetic Compton scattering because the electron energy is quantized in states with energy

$$E_n = (m^2 + p^2 + 2nB'm^2)^{1/2} , \tag{1}$$

where p is the momentum parallel to the field, $B' \equiv B/B_{cr}$ is the field strength expressed in units of the critical field, $B_{cr} = 4.414 \times 10^{13}$ G, and $n = 0, 1, 2, \ldots$ is the Landau state principal quantum number. (We use natural units, $\hbar = c = 1$, throughout.) The electron spin is described by the quantum number $s = \pm 1$ and $n = l + \frac{1}{2}(s + 1)$, where $l = 0, 1, 2, \ldots$. Each Landau state is doubly degenerate, except for the ground state, $n = 0$, where only spin down ($s = -1$) is allowed.

The different conventions for the electron wave-function solutions to the Dirac equation which have appeared in the literature can give different results for spin-dependent cross sections. This is because they are eigenfunctions of different spin operators. We have chosen to use the Johnson-Lippmann (1949) wave functions (see also Daugherty & Bussard 1980), which are based on solutions in a Cartesian coordinate frame, since they are somewhat simpler. Although other choices of wave function describe spin states that are more physically meaningful (Melrose & Parle 1983), final results which are summed over electron spin are independent of the choice of wave function. Furthermore, all wave functions are equivalent in the electron rest frame ($p = 0$), and differences in the squared matrix elements appear only in second order in p.

2.1. *Absorption*

The relativistic cross section for absorption by electrons in a strong magnetic field was derived by Daugherty & Ventura (1978). They assume that the electrons are initially in the ground state, and the expression they give is summed over the two possible final spins of the electrons in excited states following absorption. Their final expressions have made use of the energy δ-function to integrate over electron parallel momenta. For the purpose of comparing the absorption cross section to that of scattering and to include natural line width, it is more convenient to use the cross section in the electron rest frame. The result of a derivation of the rest frame cross section for absorption of a photon of energy ω and angle θ by an electron initially in the ground state ($n = 0$, $s = -1$) and finally in state n with spin-up ($i = 1$) or spin-down ($i = 2$) is

$$\sigma_{\rm abs}^{n;i}(\theta) = \frac{2\alpha\pi^2\hbar^2c^2}{\omega E_n(E_n + m)}\,\delta(E_n - m - \omega)\,\frac{e^{-Z}Z^{n-1}}{(n-1)!}\,\kappa_i^n(\theta) , \tag{2}$$

$$\kappa_1^n(\theta) = \left[\frac{Z}{n}\,2nB'm^2(\sin^2\theta, 0) + \omega^2\cos^2\theta(\cos^2\theta, 1) + \sqrt{2ZB'}\,m\omega\cos\theta(2\cos\theta\sin\theta, 0)\right] ,$$

$$\kappa_2^n(\theta) = \left[\frac{Z}{n}\,\omega^2\cos^2\theta(\sin^2\theta, 0) + 2nB'm^2(\cos^2\theta, 1) - \sqrt{2ZB'}\,m\omega\cos\theta(2\cos\theta\sin\theta, 0)\right] ,$$

where

$$Z \equiv \frac{\omega^2\sin^2\theta}{2mB'} , \tag{3}$$

and

$$E_n = (m^2 + \omega^2\cos^2\theta + 2nB'm^2)^{1/2} . \tag{4}$$

The angular factors in parentheses refer to two incident linear photon polarizations, ($\parallel$, $\perp$) to the plane containing the photon wavevector and the magnetic field. The energy δ-function requires the incident photon energy to have only one value (i.e., the resonance energy) given by

$$\omega_n = m[(1 + 2nB'\sin^2\theta)^{1/2} - 1]/\sin^2\theta . \tag{5}$$

Note that the cross section for absorption with a spin flip, $\sigma_{\rm abs}^{n;1}$, is much smaller than the cross section for absorption without a change of spin, $\sigma_{\rm abs}^{n;2}$, by a factor nB'.

We can obtain a particularly simple expression for the total absorption cross section by summing equation (2) over final spin state and averaging over photon polarization:

$$\sigma_{\rm abs}^n(\theta) = \frac{\alpha\pi^2\hbar^2c^2}{E_n}\,\delta(E_n - m - \omega)\,\frac{e^{-Z}Z^{n-1}}{(n-1)!}\left[(1 + \cos^2\theta) + \frac{Z}{n}\sin^2\theta\right] . \tag{6}$$

One can easily obtain the classical absorption cross section (Fenimore et al. 1988) from the above expression in the limit $nB' \ll 1$, where $\omega \approx nB'm$, $Z \approx n^2B'\sin^2\theta/2 \ll 1$, and $E_n \approx m$,

$$\sigma_{\rm abs}^n(\theta) \approx \frac{\alpha\pi^2\hbar^2c^2}{m}\,\delta(\omega - nB'm)\left(\frac{n^2}{2}B'\sin^2\theta\right)^{n-1}\frac{(1 + \cos^2\theta)}{(n-1)!} . \tag{7}$$

Due to the finite lifetime of electrons in excited states, the cross section for absorption does not really behave as a δ-function, but has a natural line width equal to the decay rate of the final electron state. The usual prescription for including the finite line width is to replace the δ-function in the cross section by a normalized Lorentz profile (e.g., Wasserman & Salpeter 1980). In the relativistic

case, the profiles are spin dependent,

$$L_{n,i}(\omega) = \frac{\Gamma_{n,s}/2\pi}{(\omega - \omega_n)^2 + \Gamma_{n,s}^2/4}, \tag{8}$$

where the width $\Gamma_{n,s}$ is the decay rate from state (n, s). The expression for the total absorption cross section including natural line width is therefore

$$\sigma_{\rm abs}^{n}(\omega, \theta) = L_{n,1}(\omega)\sigma_{\rm abs}^{n,1} + L_{n,2}(\omega)\sigma_{\rm abs}^{n,2} . \tag{9}$$

Note that the only ω dependence in $\sigma_{\rm abs}^{n}(\omega, \theta)$ is in the Lorentz profiles.

We use the relativistic cyclotron transition rates (Sokolov & Ternov 1968; Harding & Preece 1987) between states (n, s) and (n', s') to determine the decay rates:

$$\Gamma_{n,s} = \sum_{n'=0}^{n-1} \sum_{s'} \Gamma_{n,n';s,s'} . \tag{10}$$

Since we have used Johnson-Lippmann wave functions to calculate the absorption cross section, we must be careful to use the same spin convention for the cyclotron transition rates, although the choice of gauge need not be the same. This is important because the decay rates should be evaluated for arbitrary parallel momentum of the excited state, which we know from momentum conservation is $p = \omega_n \cos\theta$. We use expressions given by Sokolov & Ternov (1968, p. 68) for the cyclotron transition rates based on electron wave function solutions in a cylindrical coordinate gauge, but which are eigenfunctions of the same spin operator as are the Johnson-Lippmann wave functions.

2.2. *Scattering*

The complexity of the second-order scattering cross section is due to the presence of an infinite sum over virtual intermediate states which need not satisfy energy conservation. It is a physically more accurate description of resonant scattering than first-order absorption, which only describes scattering for which energy is conserved in the intermediate state. Herold (1979) derived the relativistic scattering cross section for electrons both initially and finally in the ground state. Several other derivations have included scattering to arbitrary excited states (Daugherty & Harding 1986, hereafter DH; Bussard, Alexander, & Mészáros 1986). We will calculate the scattering cross section including the relativistic natural line widths using the results of DH.

In the electron rest frame, the cross section for scattering from initial state 0 to final state l takes the form

$$\frac{d\sigma_{\rm sc}^{0,l;s'}(\omega, \theta)}{d\Omega'} = \frac{3}{4}\sigma_{\rm T}\frac{\omega'}{\omega}\frac{e^{-(k_\perp^2 + k_\perp'^2)/2mB'}}{[m + \omega - \omega' - (k_z - k_z')\cos\theta']}\left|\sum_{n=0}^{\infty}\sum_{i=1}^{2}(F_{n,i}^{(1)}e^{i\Phi_1} + F_{n,i}^{(2)}e^{i\Phi_2})\right|^2 , \tag{11}$$

where $k^\mu = (\omega, \boldsymbol{k})$ and $k'^\mu = (\omega', \boldsymbol{k}')$ are the incident and scattered photon momentum four-vectors, and $\Phi_1 = -\Phi_2 = (k_\perp k_\perp'/2mB')\sin(\phi - \phi')$. The infinite sum is carried out over intermediate states with principal quantum number n. In practice, this sum converges rapidly above $n \simeq l$, with the most important contribution coming from the $n = l + 1$ resonant term. The $F_{n,i}^{(1)}$ and $F_{n,i}^{(2)}$ refer to the two possible second-order diagrams (see DH), which are related through crossing symmetry. Their full expressions are given in the Appendix. The scattered photon energy, ω', is determined from kinematics by the incident photon energy and the incident and scattered photon angles.

$$\omega' = \{m + \omega(1 - \cos\theta\cos\theta') - [m^2 + 2m\omega\cos\theta'(\cos\theta' - \cos\theta) + \omega^2(\cos\theta' - \cos\theta)^2 + 2lm^2B'\sin^2\theta']^{1/2}\}/\sin^2\theta' . \tag{12}$$

Calculation of the total scattering cross section therefore consists of an integration of equation (11) over the scattered photon solid angle.

The resonances in the scattering cross section arise in $F_{n,i}^{(1)}$ from expressions of the form $(m + \omega - E_n)$ in the denominator of terms for the electron intermediate states of energy E_n. Similarly, expressions of the form $(m + \omega + E_n)$ are present in the denominator of terms for positron intermediate states. To include natural line widths, one makes the replacement

$$E_n \rightarrow E_n - \frac{i\Gamma_{n,s}}{2} , \tag{13}$$

where we use the relativistic decay rate corresponding to the nth intermediate state. As in the case of absorption, the decay rates for the scattering cross section are evaluated with the parallel momentum, $P = \omega\cos\theta$, of the intermediate state.

2.3. *Nonrelativistic Limit*

It is interesting to examine the behavior of the spin-dependent absorption cross section in the nonrelativistic limit. Expanding equation (2) to first order in nB' and averaging over photon polarization, we have

$$\sigma_{\rm abs}^{n,1}(\theta) \simeq \frac{\alpha\pi^2\hbar^2c^2}{2m}\frac{nB'}{(n-1)!}\left(\frac{n^2}{2}B'\sin^2\theta\right)^{n-1}(1 + \cos^2\theta) ,$$

$$\sigma_{\rm abs}^{n,2}(\theta) \simeq \frac{\alpha\pi^2\hbar^2c^2}{m(n-1)!}\left(\frac{n^2}{2}B'\sin^2\theta\right)^{n-1}[(1 + \cos^2\theta) - 2nB'\sin^2\theta\cos^2\theta] . \tag{14}$$

The nonrelativistic limits of the spin-dependent decay rates from state n take the form (Herold, Ruder, & Wunner 1982)

$$\Gamma_{n,1} \simeq \tfrac{4}{3}\alpha m B'^2 (n-1), \qquad n > 1,$$
$$\simeq \tfrac{2}{3}\alpha m B'^3, \qquad n = 1; \tag{15}$$
$$\Gamma_{n,2} \simeq \tfrac{4}{3}\alpha m B'^2 n. \tag{16}$$

Evaluating the total cross section from equation (9), including the spin-dependent natural line width, at the first harmonic ($n = 1$),

$$\sigma^1_{\rm abs} = \sigma^{1,1}_{\rm abs}\frac{2}{\pi\Gamma_{1,1}} + \sigma^{1,2}_{\rm abs}\frac{2}{\pi\Gamma_{1,2}}$$
$$\simeq \frac{\pi\hbar^2c^2}{m^2B'^2}\,3(1+\cos^2\theta), \tag{17}$$

which is exactly twice the result of evaluating the classical absorption cross section (eq. [7]) at the first harmonic using the nonrelativistic decay rate expression (eq. [16]). Even though the spin-up absorption cross section $\sigma^{1,1}_{\rm abs}$ is smaller by one power of B' than the spin-down cross section $\sigma^{1,2}_{\rm abs}$, the decay rate of the spin-up state is also smaller by B'. The two spin states thus give equal contributions to the cross section at the resonance energy. At low values of nB', the contribution to absorption from the spin-up state is a δ-function at ω_n and therefore has a negligible effect on line profiles. As nB' approaches 1 the δ-function will broaden into a narrow Lorentz profile superposed on the broader profile of the spin-down state.

3. COMPARISON OF SCATTERING AND ABSORPTION

We have calculated the polarization-averaged absorption cross section (eqs. [2] and [9]) and the total scattering cross section, obtained by integrating equation (11) over final photon angles and summing over final electron state l, for the first four harmonics, at incident photon angles $\theta = 30°$, 60°, 85° and magnetic field strengths $B = 1.7 \times 10^{12}$ G ($B' = 0.0385$), $B = 4.4 \times 10^{12}$ G ($B' = 0.1$), and $B = 10^{13}$ G ($B' = 0.226$). Figure 1 shows a comparison of the total absorption and scattering cross sections for $B' = 0.1$ and $\theta = 30°$. On this scale, the visible difference is due primarily to nonresonant scattering terms which enhance the cross section between resonances and can be significant at higher, weaker harmonics. This will have more of an effect at lower fields and smaller θ, where resonance peaks at higher harmonics decrease faster relative to the continuum. However, some difference in the resonance structure is also apparent: although the two cross sections agree to second order in α at the resonance energies, the scattering cross section falls off more quickly on the red side and more slowly on the blue side of the resonance peaks. This behavior is due to the ω-dependence in the numerator of the resonant scattering terms. Because of energy and momentum conservation, ω-dependence in the absorption cross section appears only in the denominator of the Lorentz profile.

Figure 2 shows the ratio of the scattering to absorption cross section as a function of incident photon energy and angle. The increase of this ratio away from the resonance energies, where it is very close to 1, is gradual at the first harmonic but steeper at higher harmonics. At angles other than 90° there is a particularly sharp increase on the scale of the resonance width. The behavior of the scattering to absorption ratio near the resonance peaks can be seen more clearly in Figure 3, where we plot the relative difference

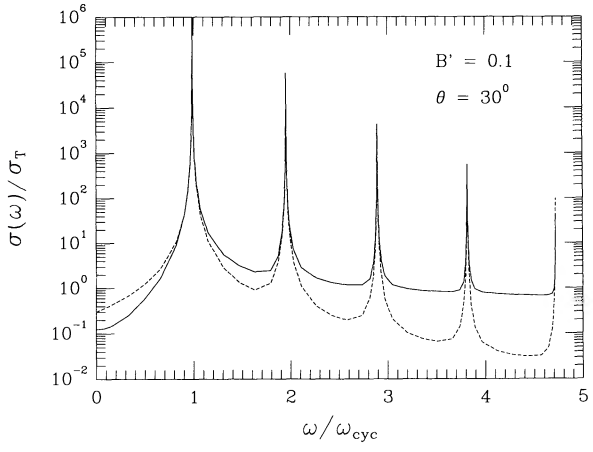

FIG. 1

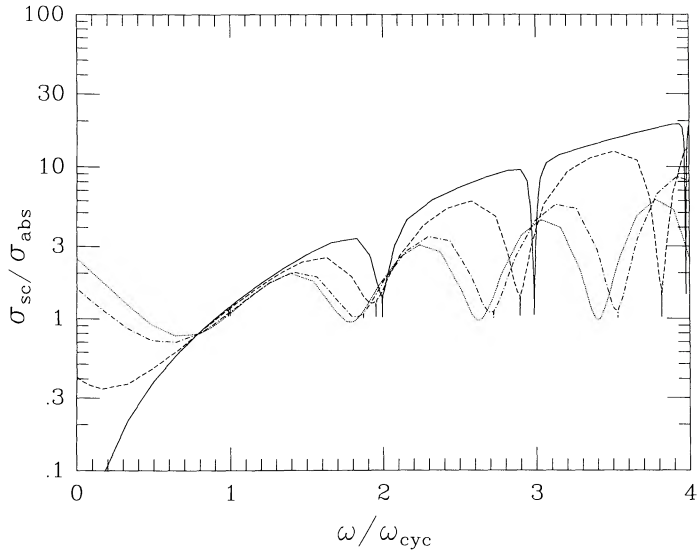

FIG. 2

FIG. 1.—Scattering (*solid line*) and absorption (*dashed line*) cross sections with spin-dependent relativistic natural line width as a function of incident photon energy (in units of the cyclotron energy) for field strength $B' = 0.1$ and photon angle $\theta = 30°$.

FIG. 2.—Ratio of scattering and absorption cross sections as a function of incident photon energy at different angles θ to the magnetic field, $B = 4.4 \times 10^{12}$ G: 10° (*solid line*), 30° (*dashed line*), 60° (*dot-dashed line*), and 90° (*dotted line*).

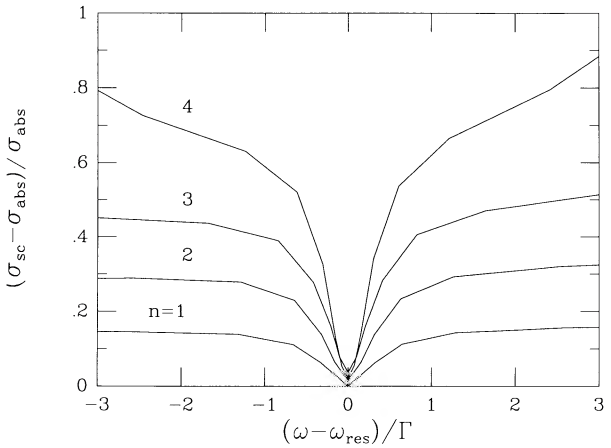

FIG. 3.—Relative difference between scattering and absorption cross sections as a function of the number of natural line widths away from resonance, $(\omega - \omega_{res})/\Gamma$, for field strength $B = 4.4 \times 10^{12}$ G and $\theta = 30°$. Curves are labeled with the value of the harmonic number n.

$|(\sigma_{sc} - \sigma_{abs})/\sigma_{abs}|$ versus the number of widths away from resonance $(\omega - \omega_n)/\Gamma_n$, with Γ_n approximated by the nonrelativistic decay rate (eq. [16]). The sharp increases indeed occur on the scale of the resonance width and $|(\sigma_{sc} - \sigma_{abs})/\sigma_{abs}|$ becomes relatively constant beyond one width from resonance. Figure 4 shows how the value of $(\sigma_{sc} - \sigma_{abs})/\sigma_{abs}$ at $|(\omega - \omega_n)| = \Gamma_n$ increases as a function of field strength, harmonic number, and cos θ. Even at field strength $B' = 0.0385$, the absorption cross section as given by equation (9) is not accurate at small angles to the field, especially above the first harmonic.

The above dependence can be understood by examining the resonance profile of the scattering cross section and comparing it to

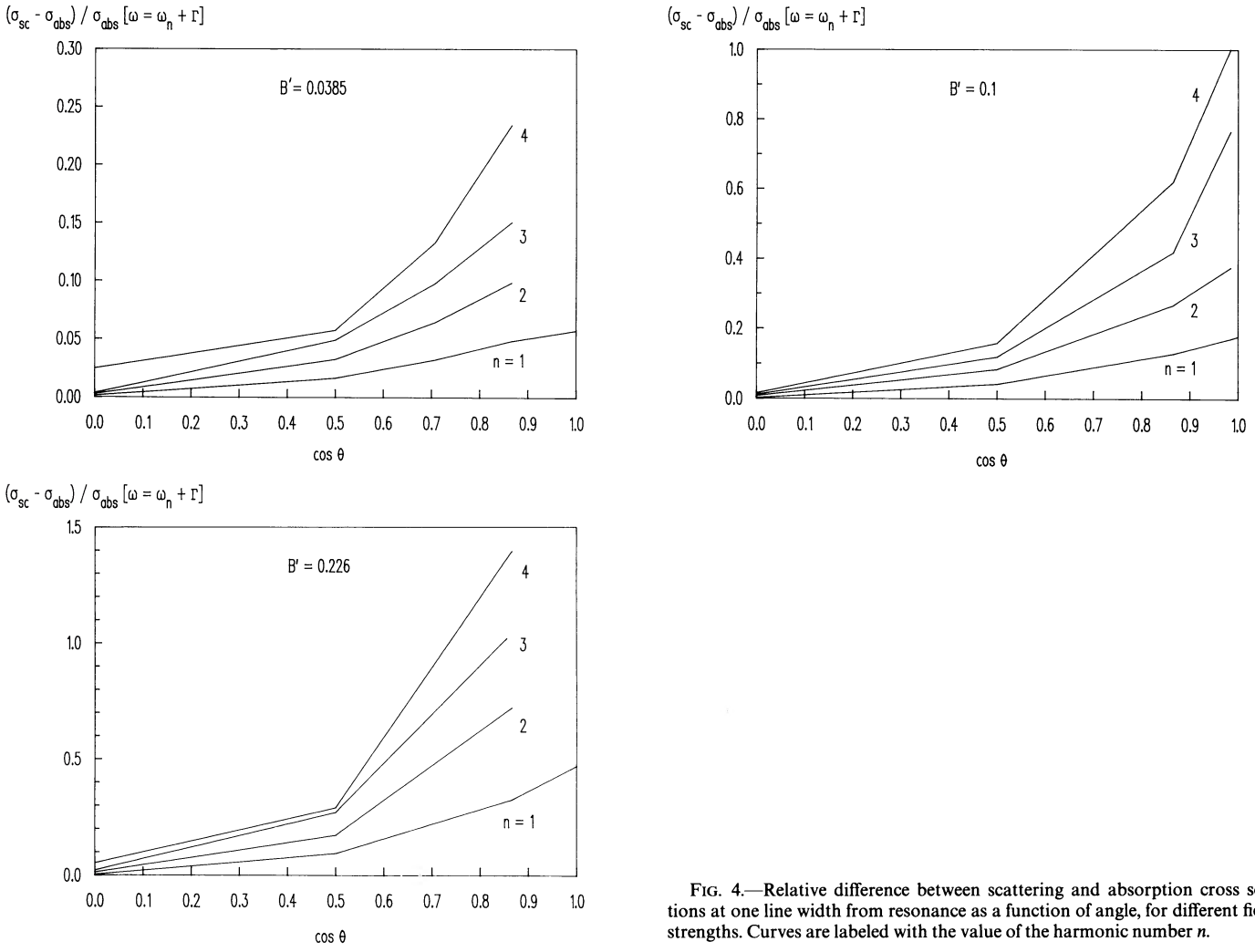

FIG. 4.—Relative difference between scattering and absorption cross sections at one line width from resonance as a function of angle, for different field strengths. Curves are labeled with the value of the harmonic number n.

the Lorentz profile of the absorption cross section. The resonant terms in the scattering cross section come from combining intermediate state electron and positron terms (cf. eqs. [A1]–[A4]) to form the common denominator,

$$\left(m + \omega + E_n - \frac{i\Gamma_n}{2}\right)\left(m + \omega - E_n + \frac{i\Gamma_n}{2}\right) = (2m\omega + \omega^2 \sin^2\theta - 2m^2nB') + iE_n\Gamma_n + \frac{\Gamma_n^2}{4}, \tag{18}$$

where E_n is given by equation (4). The resonance energy (eq. [5]) is the root of the term in parentheses on the right-hand side. Terms with $n = 0, 1, 2, \ldots, \infty$ are summed in the cross section, but for ω near the nth resonance energy, only the nth term in the sum is important.

Considering only the nth resonant term and taking the square modulus as it finally appears in the cross section, we have

$$\left(\omega + \frac{\omega^2 \sin^2\theta}{2m} - nB'm\right)^2 + \left(\frac{E_n\Gamma_n}{2m}\right)^2, \tag{19}$$

where we have dropped the Γ_n^2 term in equation (18). Since the resonant scattering and absorption cross sections are equal at the resonance, we can derive the approximate form of the scattering resonant profile by normalizing to absorption at $\omega = \omega_n$:

$$\sigma_{sc} \simeq A_n \frac{E_n^2\Gamma_n/2\pi m^2}{(\omega + \omega^2 \sin^2\theta/2m - nB'm)^2 + (E_n\Gamma_n/2m)^2}, \tag{20}$$

where $A_n \equiv \sigma_{abs}/L_n$. Expanding the above profile at $\omega = \omega_n + \Gamma_n$ to first order in nB', we find that

$$\left.\frac{(\sigma_{sc} - \sigma_{abs})}{\sigma_{abs}}\right|_{\omega=\omega_n+\Gamma_n} \simeq \frac{8}{5} nB' \cos^2\theta, \tag{21}$$

which is an excellent approximation to the actual dependence of the cross sections for the parameter space we are considering.

It thus appears that the standard Lorentz profile used to describe the natural line-width broadening of the absorption resonance is inaccurate at photon energies where relativistic corrections become important, that is, when $nB' \sim 1$. There are essentially two corrections to the nonrelativistic Lorentz profile that are evident in equation (20). The first is the different form in which the relativistic cyclotron energy (see eq. [5]) appears in the denominator, and the second is an increase in the natural line width of the excited electron state by the factor E_n/m. This factor is not a time dilation gamma factor because the decay rate is already evaluated in the laboratory frame. Furthermore, the time dilation of the rest-frame decay rate would be $\Gamma_n(p) = [m(1 + 2nB')^{1/2}/E_n]\Gamma_n(p = 0)$ (Herold, Ruder, & Wunner 1982). These corrections are first order in α since they appear in the resonant part of the cross section. The strong angular dependence comes from the parallel momentum, $\omega \cos\theta$, of the intermediate state. The above results suggest that a much more accurate approximation to resonant scattering would follow from replacing the Lorentz profiles in the absorption cross section equation (9) by the profile given in equation (20).

4. LINE PROFILES

The line profiles corresponding to absorption or resonant scattering are given by

$$\phi(\omega, \mu) = \sum_n \int_{-\infty}^{\infty} dp\, f(p)\sigma_R^n(\omega_R, \mu_R)(1 - \beta\mu), \tag{22}$$

where $\sigma_R^n(\omega_R, \mu_R)$ is the appropriate cross section, $\mu = \cos\theta$, and $f(p)$ denotes the longitudinal momentum distribution function for the electrons, all of which are assumed to be initially in the lowest Landau level. The label "R" on the cross sections indicates that they are to be evaluated in the frame in which the electron is initially at rest.

Using the absorption and scattering cross sections described in § 2, we have performed fully relativistic numerical calculations of line profiles for thermal electrons with relativistic one-dimensional Maxwellian distributions of the form

$$f(p) = C \exp\left[-(E_0 - m)/kT\right], \tag{23}$$

where T is the (longitudinal) electron temperature, $E_0 = (m^2 + p^2)^{1/2}$, and C is a normalization constant ($\int_{-\infty}^{\infty} f(p)dp = 1$). Since the integrand in equation (22) tends to be a sharply peaked function of p, especially for low values of kT, we have used an adaptive Simpson integration algorithm with relative error tolerances for the numerical calculation of the profiles.

In evaluating the absorption profiles, the rest-frame cross section may be computed for each value of p in equation (22). Calculation of the scattering cross section, however, is too time-consuming to evaluate in this way. For the scattering profiles, we interpolate from two-dimensional tables of computed cross section values in a grid of rest-frame ω_R and μ_R. The ω_R resolution of the tables is variable, with finest resolution near the resonant peaks, and we have used angles, 0°, 10°, 30°, 60°, 90°. At each ω value in the profile, the p integration traces a curve in the ω_R–μ_R plane. In order to improve the interpolation along this curve near the resonance peaks, we convert all ω_R values to a new coordinate,

$$\omega_I = \frac{(\omega_R \sin^2\theta/m + 1)^2 - 1}{2B' \sin^2\theta}, \tag{24}$$

which is obtained by inverting the resonance formula (eq. [5]). Using ω_I and μ_R as coordinates eliminates inaccuracies due to the shift of resonance energy with μ_R, because we are effectively interpolating at nearly constant "elevation" along the resonance ridges.

The results, shown in Figures 5–7, reveal the characteristic dependencies of the profiles on the three physical parameters of

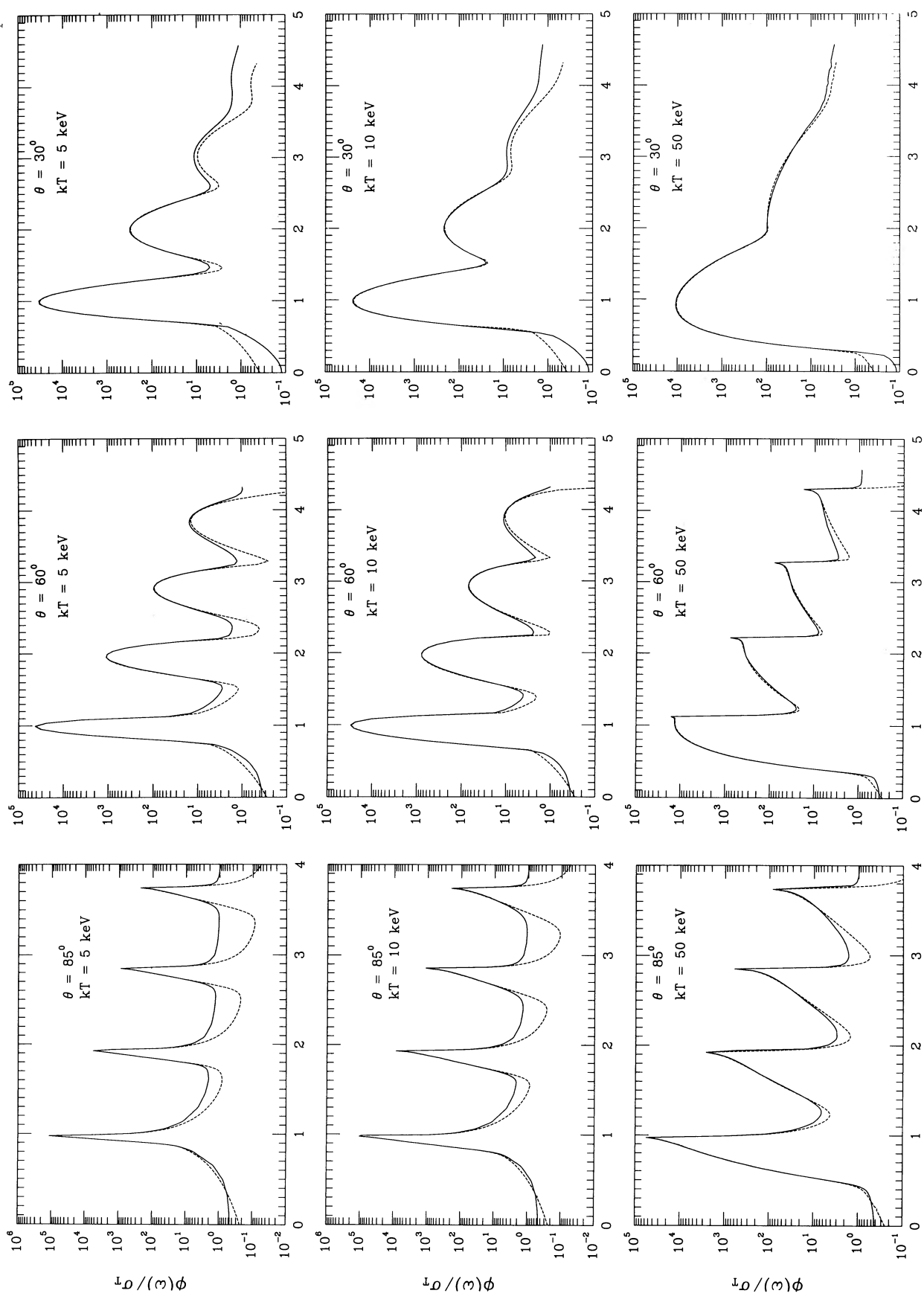

FIG. 5.—Scattering (*solid line*) and absorption (*dashed line*) profiles, $\phi(\omega, \mu)$, in units of the Thomson cross section at various photon angles, θ, and electron parallel temperatures, kT, for a magnetic field strength $B = 1.7 \times 10^{12}$ G.

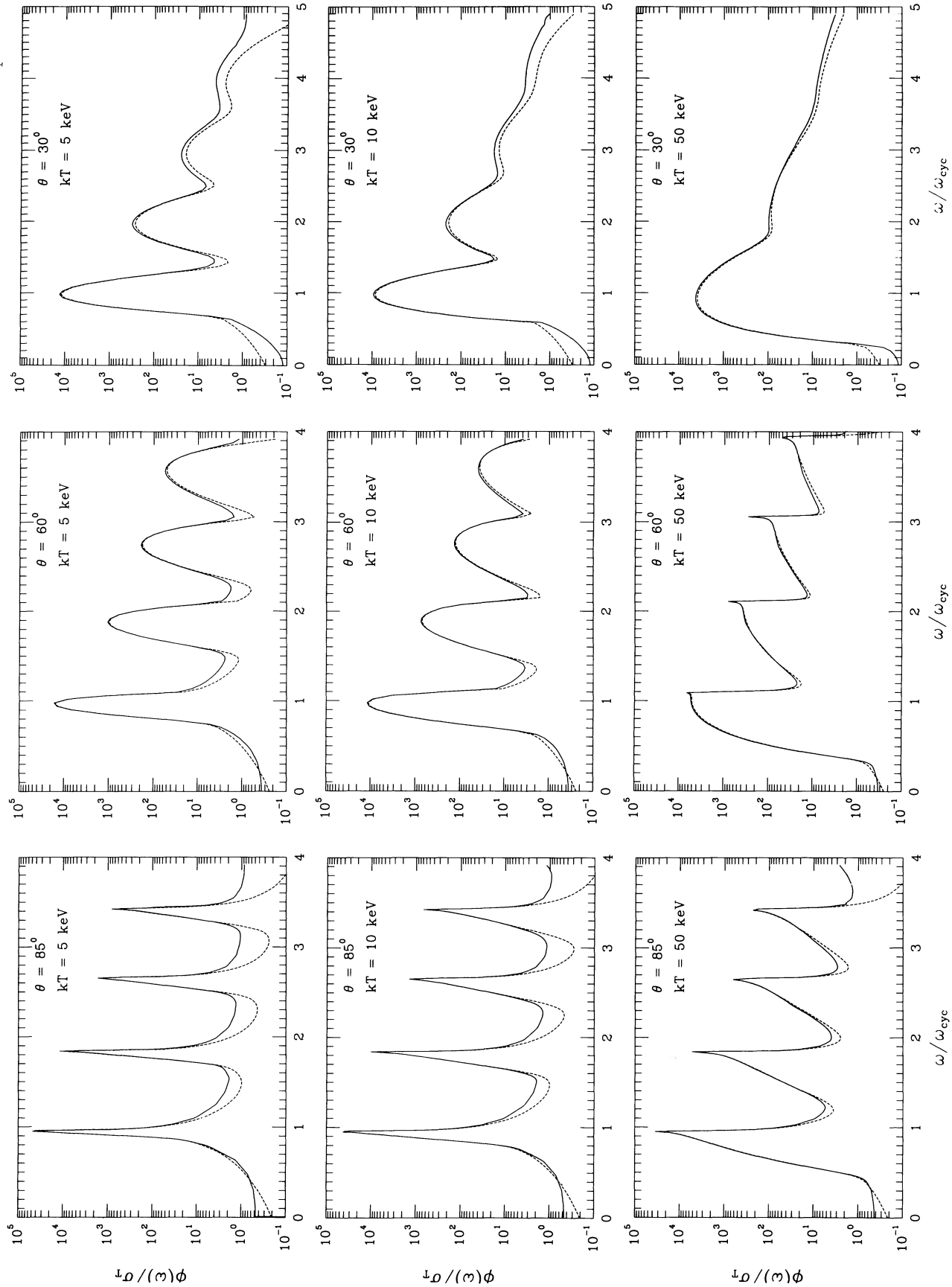

FIG. 6.—Same as Fig. 5, for a magnetic field strength $B = 4.4 \times 10^{12}$ G

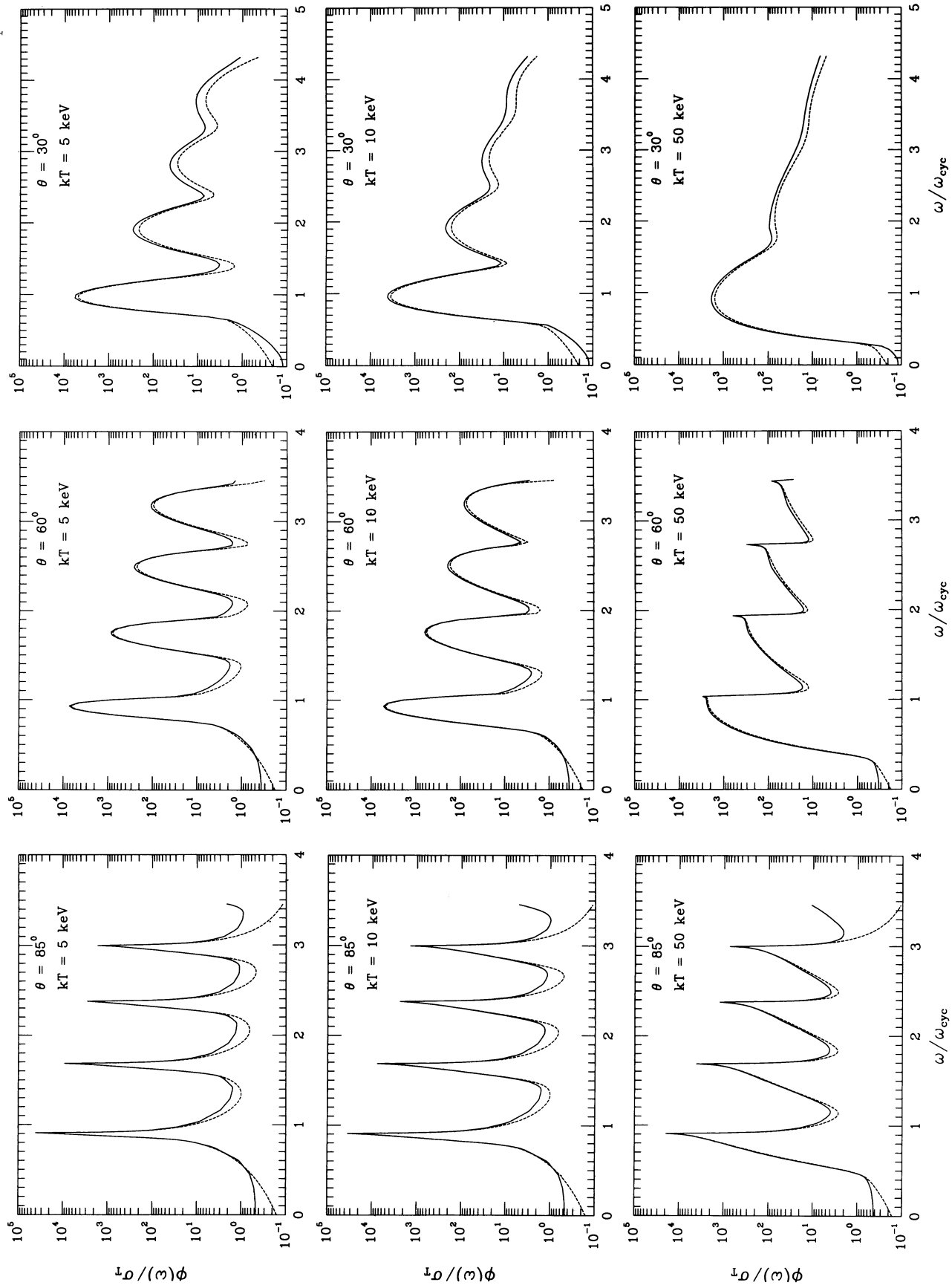

FIG. 7.—Same as Fig. 5, for a magnetic field strength $B = 10^{13}$ G

interest, namely magnetic field strength B, photon angle of incidence (measured with respect to B), and longitudinal electron temperature T. The range of B considered here is 1.7–10 TG, where the lower limit is motivated by recent observations of line features in two gamma-ray bursts (Murakami et al. 1988). The temperature range extends from 5–50 keV.

4.1. *Structure of the Resonance Peaks*

Perhaps the most obvious aspect of these figures is that the general shapes of the profiles for scattering and absorption are quite similar near the resonance peaks and in fact show significant differences only in the wings and below the first resonance. This similarity shows that the structure of the peaks is determined by relativistic kinematical effects (Daugherty & Ventura 1978; Wang & Lamb 1990), since the kinematics of first-order absorption and second-order scattering are identical at the resonances.

In order to explain the details of the peak structure, it is useful first to give a concise review of relativistic absorption kinematics. Since the profiles are formed by a distribution of incident electron momenta p, the kinematical equations must be written for the general case of nonzero p,

$$p' = p + \omega \cos\theta ,$$
$$E_n = E_0 + \omega . \tag{25}$$

The resonance energies (eq. [5]) are, of course, obtained by solving equation (25) for ω_n with $p = 0$. However, for arbitrary choices of ω, θ, B, and final-state number n, equation (25) may be satisfied by either 2, 1, or 0 values of p. As noted by Daugherty & Ventura (1978), the solutions for p satisfy the equation, $f_1(p) = f_2(p)$, where

$$f_1(p) = (p^2 + m^2)^{1/2} , \tag{26}$$

$$f_2(p) = p\cos\theta + nB'\frac{m^2}{\omega} - \frac{\omega}{2}\sin^2\theta . \tag{27}$$

Figure 8 illustrates geometrical solutions for p defined by the intersections of equations (26) and (27), which can serve to explain certain aspects of the line shapes. In particular, the special cases in which only one solution for p exists correspond to the high-energy cutoffs seen at or above the resonance energies in the profile plots. The cutoff energies are given by

$$\omega^n_{\max} = \frac{m[(1 + 2nB')^{1/2} - 1]}{\sin\theta} , \tag{28}$$

which shows that the cutoffs coincide with the resonance energies for $\mu = 0$ and become greater than ω_n as μ increases.

For pure absorption (neglecting decay rates), the cross sections are singular at the cutoff energies. Decreasing ω below the cutoffs (while keeping the other parameters fixed) raises the intercept of the straight line in Figure 8, yielding two solutions for p. The height of the profile peak at any given energy below the cutoff is then determined by the values of the distribution function $f(p)$ at the two p-solutions. [Note that for $\mu \neq 0$, the peaks can have smooth local maxima below the cutoffs, at the photon energy for which one of the p-solutions reaches the maximum of $f(p)$ at $p = 0$.]

Because of these kinematical effects, the variation of the line profiles with photon incidence angle is more complicated than the dependence on either field strength or temperature. In particular, equation (5) shows that the spacing between resonances increases with decreasing incidence angle, while equation (28) shows that the cutoff energies are increased by even larger amounts. Moreover, since μ is the slope of the straight line in Figure 8, the p-solutions of equations (26) and (27) (and hence the shape of the profile peaks) exhibit a complicated dependence on incidence angle.

Compared to the dependence of the profiles on photon incidence angle, the variation with field strength and temperature are fairly straightforward. The principal effect of increasing B (for fixed μ and T) is to reduce each resonance energy (5) and cutoff energy (28) from its nonrelativistic limit, but the relative shifts are smaller than the shifts induced by varying μ. Since the amount of these

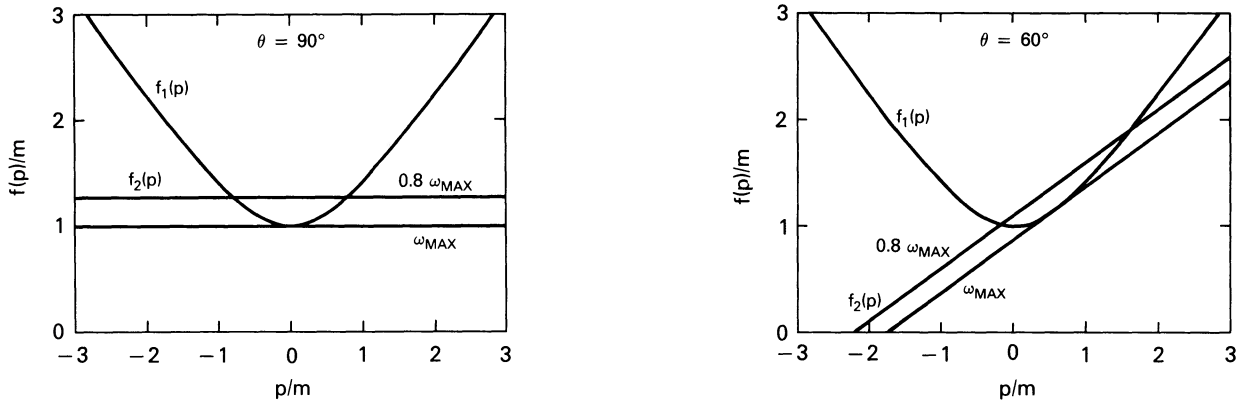

FIG. 8.—Examples of electron momentum, p, solutions which satisfy the simultaneous one-dimensional kinematic equation (25) for two different angles to the magnetic field ($B = 4.4 \times 10^{12}$ G). In the figure, $f_2(p)$ is evaluated at the first harmonic cutoff energy, $\omega_{\max}$ (eq. [28]) and at $\omega = 0.8\omega_{\max}$.

redshifts increases with harmonic number n, the spacing between successive resonance peaks becomes increasingly compressed. The dependence on T is even simpler, since in this case there are no shifts in either the resonance or cutoff energies. The principal effect of increasing T is just to broaden the peaks on both sides of the resonance energies, but only up to the cutoffs on the high-energy side. The cutoff energy can become more apparent in the profile with increasing T from this effect (as can be seen in the $\theta = 60°$, $kT = 50$ keV profiles in Figs. 5–7).

Based on the difference between the shape of the absorption and scattering cross sections near the resonance discussed in § 3, we would expect a difference in the values of the absorption and scattering profiles at the resonance. This is evident in Figures 5–7, where the values of the scattering profiles at resonance exceed those of the absorption profiles by an amount that increases with decreasing θ and increasing B and n. We can derive the approximate dependence on the relative difference in the profiles at ω_n as the relative difference of the integrated Lorentz profiles for absorption (eq. [8]) and scattering (eq. [20]), assuming the electron distribution function is slowly varying over the Lorentz width:

$$\frac{\phi_{sc}(\omega_n, \mu) - \phi_{abs}(\omega_n, \mu)}{\phi_{abs}(\omega_n, \mu)} \simeq nB'\mu^2 . \tag{29}$$

The above approximation breaks down at combinations of B', n, and μ where nonresonant scattering contributions become important. For example, nonresonant contributions are important at $n = 3$ and 4, $B_{12} = 1.7$ and $\theta = 30°$ in Figure 5, and cause the relative difference in scattering and absorption profiles to be much larger than predicted by equation (29). Figure 9 shows the effect on the absorption line profile of using the resonant scattering profile given in equation (20) in place of the standard Lorentz profile (eq. [8]) in the absorption cross section. Even in the highest field, smallest angle case of Figures 5–7, this prescription corrects nearly all of the discrepancy between scattering and absorption profiles.

4.2. *Structure in the Wings*

The structure of the profiles far from the resonance energies is determined by the Lorentz profile and, in the case of scattering, nonresonant contributions. The overall shape is a combination of the Doppler broadening profile and the Lorentz profile. In the case of nonrelativistic kinematics, the Doppler profile is Gaussian and dominates the profile shape near the resonance, but it falls off faster than the Lorentz profile, which dominates in the wings. This so-called Voigt profile has been discussed by Wasserman & Salpeter (1980). In the relativistic case, the behavior is more complicated and becomes very angle dependent. For small θ, the behavior is much like the nonrelativistic case, whereas for θ near 90° the Lorentz shape determines the profile shape much closer to the resonance since it competes only with the second-order Doppler broadening. At higher temperatures, Doppler broadening is relatively more important at all angles. Likewise, the nonresonant contributions to the scattering profile are more important in determining profile shape at angles near 90°.

5. DISCUSSION

We have quantitatively examined the accuracy of the first-order absorption description of cyclotron resonant scattering in a strong magnetic field. To obtain results that are relativistically correct, it is necessary to have a spin-dependent description of both cross sections. The spin-dependent expressions are given here for both the absorption and scattering cross sections. When the relativistic decay rates are included, we find agreement between the absorption and scattering cross sections at the resonance energies. As the photon energy moves away from resonance, the absorption cross section with a standard Lorentz profile falls below the scattering cross section. It is found that the main contribution to the difference, which can be significant within one natural line width from resonance, is that the relativistic resonant scattering profile is not a standard Lorentzian. The main results of the paper are equation (20), which gives an approximation to the relativistic scattering profile, and equation (29), which gives an approximation to the error in the absorption line profile at the resonance energy resulting from the difference in the cross sections. Use of

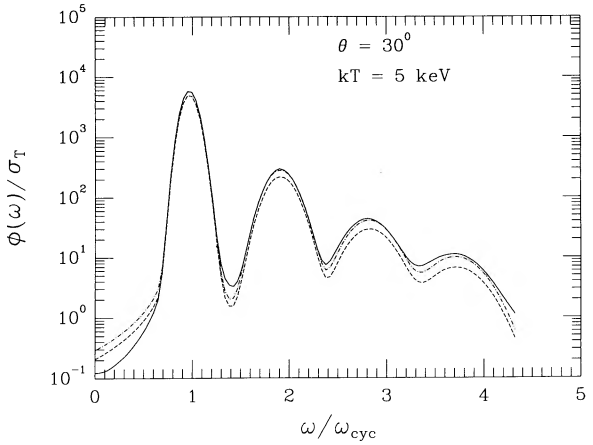

FIG. 9.—Comparison of scattering (*solid line*), absorption with a standard Lorentz profile (*dashed line*), and corrected absorption (*dot-dashed line*) profiles, $\phi(\omega, \mu)$, in units of the Thomson cross section at magnetic field strength $B = 10^{13}$ G.

equation (20) in place of the Lorentz profile in the absorption cross section will give line profiles that are much closer to the scattering line profiles.

As these results apply to models of cyclotron line formation in astrophysical sources, the difference between the scattering and absorption descriptions only become important at the first two harmonics in magnetic fields above $0.1B_{cr}$. However, at the third harmonic and above, the difference is important even in low fields due to the contribution from nonresonant scattering. This is especially true at small angles to the field, where the resonances in the cross section are weakening very quickly with increasing harmonic number. This could make a difference in determining the unknown angle to the field through fitting observed line spectra to calculated ones. For example, in the case of *Ginga* burst GB 880205, which has a field strength $B = 1.7 \times 10^{12}$ G as inferred from the line energies, the nonresonant scattering contribution is significant in predicting the strength of the third harmonic at small θ. Another effect to be noted is that the resonant profile of the scattering cross section has an effectively larger natural line width, $(E_n/m)\Gamma_n$, than the Lorentz profile. Lamb et al. (1989) point out that the natural line width is essential in the escape of resonant photons from the line core. An increase in the intrinsic line width could increase the effectiveness of resonant photon frequency redistribution and escape. This effect has been included in the calculated model spectra of Alexander & Mészáros (1989), who used the relativistic scattering cross section.

The shape of the resonant line profile is extremely sensitive to viewing angle with respect to the magnetic field, more so than to either the magnetic field strength or the temperature. This is a consequence of the one-dimensional kinematics of the scattering electrons. The relative shift of the resonance and cutoff energies resulting from changing the viewing angle is larger than the shift resulting from the same percentage change in field strength. Therefore, observed temporal variations in cyclotron line energy in a gamma-ray burst are a much better diagnostic of viewing angle than field strength. The same is true of the observed ratio of third to second harmonics.

We are grateful to D. Q. Lamb and J. Wang for comparison of profile calculations, as well as R. Preece and J. Brainerd for useful discussions.

APPENDIX

SPIN-DEPENDENT SCATTERING CROSS SECTION

The expressions for the matrix elements $F^{(1)}_{n,i}$ and $F^{(2)}_{n,i}$ of the Compton scattering cross sections in equation (11) are dependent on the total quantum number, n, and spin ($i = 1, 2$) of the electron or positron in the intermediate state. Since the expressions for the cross section given in DH were summed over intermediate state spin, we give here the expressions in the electron rest frame for the matrix elements of the separate intermediate spin states which are needed to include the spin-dependent natural line width. The "spin-flip" case, where the electron has final spin up and the "no spin-flip," final spin down, case are given separately. Evaluation of the total cross section requires a sum over final spin states.

No spin-flip:

$$F^{(1)}_{n,1} = \frac{(E_n + m)}{2E_n(m + \omega - E_n)} [(P - Q)P\epsilon'_+ \epsilon_- \Lambda_{l,n-1}\Lambda_{n-1,0} - (P - Q)N\epsilon'_+ \epsilon_z \Lambda_{l,n-1}\Lambda_{n,0} - NP\epsilon'_z \epsilon_- \Lambda_{l,n}\Lambda_{n-1,0} + N\epsilon'_z \epsilon_z \Lambda_{l,n}\Lambda_{n,0}$$
$$+ KP\epsilon'_z \epsilon_- \Lambda_{l-1,n-1}\Lambda_{n-1,0} - NK\epsilon'_z \epsilon_z \Lambda_{l-1,n-1}\Lambda_{n,0}] + \frac{(E_n + m)}{2E_n(m + \omega + E_n)} [(1 + PQ)\epsilon'_+ \epsilon_- \Lambda_{l,n-1}\Lambda_{n-1,0}$$
$$- KN\epsilon'_- \epsilon_- \Lambda_{l-1,n}\Lambda_{n-1,0} - NQ\epsilon'_z \epsilon_- \Lambda_{l,n}\Lambda_{n-1,0} - KP\epsilon'_z \epsilon_- \Lambda_{l-1,n-1}\Lambda_{n-1,0}]; \quad \text{(A1)}$$

$$F^{(1)}_{n,2} = \frac{(E_n + m)}{2E_n(m + \omega - E_n)} [(P + Q)P\epsilon'_z \epsilon_z \Lambda_{l,n}\Lambda_{n,0} + (P + Q)N\epsilon'_z \epsilon_- \Lambda_{l,n}\Lambda_{n-1,0} + NP\epsilon'_+ \epsilon_z \Lambda_{l,n-1}\Lambda_{n,0} + N\epsilon'_+ \epsilon_- \Lambda_{l,n-1}\Lambda_{n-1,0}$$
$$+ KP\epsilon'_- \epsilon_z \Lambda_{l-1,n}\Lambda_{n,0} + KN\epsilon'_- \epsilon_- \Lambda_{l-1,n}\Lambda_{n-1,0}] + \frac{(E_n + m)}{2E_n(m + \omega + E_n)} [(1 - PQ)\epsilon'_z \epsilon_z \Lambda_{l,n}\Lambda_{n,0}$$
$$+ KN\epsilon'_z \epsilon_z \Lambda_{l-1,n-1}\Lambda_{n,0} - NQ\epsilon'_+ \epsilon_z \Lambda_{l,n-1}\Lambda_{n,0} - KP\epsilon'_- \epsilon_z \Lambda_{l-1,n}\Lambda_{n,0}]. \quad \text{(A2)}$$

Spin-flip:

$$F^{(1)}_{n,1} = \frac{(E_n + m)}{2E_n(m + \omega - E_n)} [(P + Q)P\epsilon'_z \epsilon_- \Lambda_{l-1,n-1}\Lambda_{n-1,0} - (P + Q)N\epsilon'_z \epsilon_z \Lambda_{l-1,n-1}\Lambda_{n,0} + NP\epsilon'_- \epsilon_- \Lambda_{l-1,n}\Lambda_{n-1,0}$$
$$- N\epsilon'_- \epsilon_z \Lambda_{l-1,n}\Lambda_{n,0} + KP\epsilon'_+ \epsilon_- \Lambda_{l,n-1}\Lambda_{n-1,0} - NK\epsilon'_+ \epsilon_z \Lambda_{l,n-1}\Lambda_{n,0}] + \frac{(E_n + m)}{2E_n(m + \omega + E_n)} [(1 - PQ)\epsilon'_z \epsilon_- \Lambda_{l-1,n-1}\Lambda_{n-1,0}$$
$$+ NK\epsilon'_z \epsilon_- \Lambda_{l,n}\Lambda_{n-1,0} - NQ\epsilon'_- \epsilon_- \Lambda_{l-1,n}\Lambda_{n-1,0} - KP\epsilon'_+ \epsilon_- \Lambda_{l,n-1}\Lambda_{n-1,0}]; \quad \text{(A3)}$$

$$F^{(1)}_{n,2} = \frac{(E_n + m)}{2E_n(m + \omega - E_n)} [-(P - Q)P\epsilon'_- \epsilon_z \Lambda_{l-1,n}\Lambda_{n,0} - (P - Q)N\epsilon'_- \epsilon_- \Lambda_{l-1,n}\Lambda_{n-1,0} + NP\epsilon'_z \epsilon_z \Lambda_{l-1,n-1}\Lambda_{n,0}$$

$$+ N\epsilon'_z \epsilon_- \Lambda_{l-1,n-1}\Lambda_{n-1,0} - KP\epsilon'_z \epsilon_z \Lambda_{l,n}\Lambda_{n,0} - KN\epsilon'_z \epsilon_- \Lambda_{l,n}\Lambda_{n-1,0}] + \frac{(E_n + m)}{2E_n(m + \omega + E_n)} [-(1 + PQ)\epsilon'_- \epsilon_z \Lambda_{l-1,n}\Lambda_{n,0}$$

$$+ KN\epsilon'_+ \epsilon_z \Lambda_{l,n-1}\Lambda_{n,0} + NQ\epsilon'_z \epsilon_z \Lambda_{l-1,n-1}\Lambda_{n,0} + KP\epsilon'_z \epsilon_z \Lambda_{l,n}\Lambda_{n,0}] . \quad \text{(A4)}$$

$$P \equiv \frac{k_z}{E_n + m}, \qquad Q \equiv \frac{(k_z - k'_z)}{E_l + m}, \qquad N \equiv \frac{m\sqrt{2nB'}}{(E_n + m)}, \qquad K \equiv \frac{m\sqrt{2lB'}}{(E_l + m)} . \quad \text{(A5)}$$

The quantities $\Lambda_{l,n}$ and photon polarization vectors ϵ are defined in Daugherty & Harding (1986). The expressions for $F^{(2)}_{n,i}$ may be obtained directly from $F^{(1)}_{n,i}$ by the crossing symmetry replacements: $\omega \leftrightarrow -\omega'$, $\boldsymbol{k} \leftrightarrow -\boldsymbol{k}'$, and $\epsilon \leftrightarrow \epsilon'$.

REFERENCES

Alexander, S. G., & Mészáros, P. 1989, ApJ, 344, L1
Bussard, R. W., Alexander, S. B., & Mészáros, P. 1986, Phys. Rev. D, 34, 440
Bussard, R. W., & Lamb, F. K. 1982, in Gamma-Ray Transients and Related Astrophysical Phenomena, ed. R. E. Lingenfelter, H. S. Hudson, & D. M. Worrall (New York: AIP), 189
Daugherty, J. K., & Bussard, R. W. 1980, ApJ, 238, 296
Daugherty, J. K., & Harding, A. K. 1986, ApJ, 309, 362
Daugherty, J. K., & Ventura, J. 1978, Phys. Rev. D, 18, 1053
Fenimore, E. E., et al. 1988, ApJ, 335, L71
Harding, A. K., & Preece, R. D. 1989, ApJ, 338, L21
Herold, H. 1979, Phys. Rev. D, 19, 2868
Herold, H., Ruder, H., & Wunner, G. 1982, A&A, 115, 90
Heuter, G. J. 1984, in High Energy Transients in Astrophysics, ed. S. E. Woosley (New York: AIP), 373
Johnson, M. H., & Lippmann, B. A. 1949, Phys. Rev., 76, 828
Lamb, D. Q., et al. 1989, Ann. NY Acad. Sci., 571, 460
Mazets, E. P., et al. 1981, Nature, 290, 378
Melrose, D. B., & Parle, A. J. 1983, Australian J. Phys., 36, 755
Mészáros, P., Bussard, R. W., & Hartmann, D. 1986, in Gamma-Ray Bursts, ed. E. P. Liang & V. Petrosian (New York: AIP), 123
Murakami, T., et al. 1988, Nature, 335, 234
Sokolov, A. A., & Ternov, I. M. 1968, Synchrotron Radiation (New York: Pergamon)
Wang, J. C. L., et al. 1989, Phys. Rev. Letters, 63, 1550
Wang, J. C. L., & Lamb, D. Q. 1990, ApJ, submitted
Wasserman, I., & Salpeter, E. 1980, ApJ, 241, 1107